Anisotropic effects on the near-surface seismic imaging

Lina Zhang, Jie Zhang, University of Science and Technology of China; Wei Zhang, GeoTomo*

Summary

Anisotropic velocity models have been widely applied in the subsurface seismic imaging except for the near surface area. The near surface is often assumed to be isotropic, and refraction methods are applied to infer a velocity model for making seismic statics corrections. To study the effects of anisotropic media on the refractions due to HTI, which varies azimuthally, we design numerical models with anisotropic parameters assigned in the shallow layers, and perform 3D seismic raytracing with the consideration of HTI anisotropy to calculate the first-arrival traveltimes. Then we assume the near-surface area "isotropic" and invert a near-surface velocity model using isotropic traveltime tomography. It has been identified through testing that footprints of recording geometry shall be mapped to the velocity model, and velocity anomaly will be produced right above the refractor if the HTI anisotropy is ignored. By applying the azimuth dependent traveltime tomography, we could infer the fast and slow velocity models and determine the direction of the symmetry axis. We test the approach with both synthetic and real data.

Introduction

The theory of seismic anisotropy has gone through a long development. Today it becomes one of the main areas in seismic studies. Since it was first reported in exploration seismology that velocity measured on outcrops of Lorraine Shale, the direct measurement of velocity along the bedding turned out to be 40% higher than those across the bedding (McCollum and Snell ,1932) , the study of anisotropy has dramatically increased over the past two decades because of advances in parameter estimation, the transition from post-stack imaging to prestack depth migration, the wider offset and better azimuthally coverage of 3D seismic surveys, and acquisition of high-quality multi-component data. Anisotropic effects have become increasingly important in exploration. A detailed historical analysis of developments in seismic anisotropy can be found in Helbig and Thomsen (2005), Tsvankin et al., (2010).

Although it is often observed that anisotropy is weak, it does not mean that variations due to anisotropy are negligible. An interesting feature of anisotropy is that, weak anisotropy may still produce a strong influence on seismic data, consequently, on the interpretation of the data by the imaging process. In modern seismic imaging for achieving high resolution, if we ignore such effects, we may incorrectly image the subsurface.

Raytracing method

To calculate the traveltimes in the isotropic media and anisotropic media we implemented the ray tracing methods following Zhou and Greenhalgh (2005) and Bai et al., (2007) based on the shortest path method (SPM):

$$t_{ij} = \min_{i \in N_j} \left(t_i + \frac{2\left|\vec{x}_i - \vec{x}_j\right|}{U(\vec{x}_i) + U(\vec{x}_j)} \right) \tag{1}$$

Where in isotropic media $U(\vec{x}_i)$ and $U(\vec{x}_j)$ are the velocity values at the ith and the jth nodes positions, while in anisotropic media $U(\vec{x}_i)$ and $U(\vec{x}_j)$ represent the group velocities at the two different nodes.

Nonlinear traveltime tomography

A nonlinear conjugate gradient method with Gauss-Newton method was used to minimize the misfit function which leads to a matrix form that can be calculated by a computer algorithm (Zhang and Toksoz, 1998):

$$\phi(m) = (1-\omega) A_k^T \left(\vec{d} - \vec{G}(m)\right) + \omega B_k^T \left(\hat{d} - \hat{G}(m)\right) - \tau R^T R m_k \tag{2}$$

$$A \overset{def}{=} \frac{\partial \vec{G}}{\partial m} = \frac{1}{l}\frac{\partial G}{\partial m} \tag{3}$$

$$B \overset{def}{=} \frac{\partial \hat{G}}{\partial m} = \frac{\partial^2 G}{\partial m \partial x} \tag{4}$$

$$m_{k+1} = m_k + \triangle m_k \qquad k = 1, 2, 3, ..., n \tag{5}$$

where matrix A_k stores the average slowness sensitivity; B_k is the apparent slowness sensitivity matrix.

Tests of synthetic models

In this paper we test two different synthetic models with the same source and receiver geometry. The model size is given by 5000 m (X) × 5000 m (Y) × 300 m (Z). A total number of 2401 shots are set on the surface in the shape of rectangular with a spatial interval of 100m, while the receiver distribution is designed to be a circular grid in template with the offset range of 1500 m, of which the spatial interval is 50 m. The source and receiver distribution are shown in Figure 1. We test HTI anisotropic effect by using a one layer over half a space model which will help us to isolate structure effects versus anisotropic effects. During the tests two different situations are

DOI http://dx.doi.org/10.1190/segam2012-0907.1

designed, the first one is the model with HTI imposed in the half space but the top layer is free of anisotropy (Model A) while the other one is with HTI imposed in the top layer and free of anisotropy in the half a space (Model B). These two models are going to isolate the anisotropic effects due to the first layer and due to the half a space.

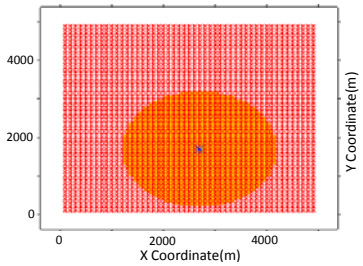

Figure 1: Source and receiver geometry for tests.

(a) 3D isotropic traveltime tomography for model A

Figure 2 shows the comparison of isotropic and anisotropic traveltimes of the model A, whose parameters are V_1=1500m/s, h_1=200m, V_2=3000m/s, ε_2=0.2, σ_2=0.1, $\eta_2=90^0$ and $\varphi_2=90^0$, where the subscript 1 represents the top layer and the subscript 2 denotes the half a space. From Figure 2 we can see that anisotropic traveltimes are faster than isotropic traveltimes at the long offsets, this is because that the long offset data are the refractions that propagate in the half a space where HTI anisotropy exists.

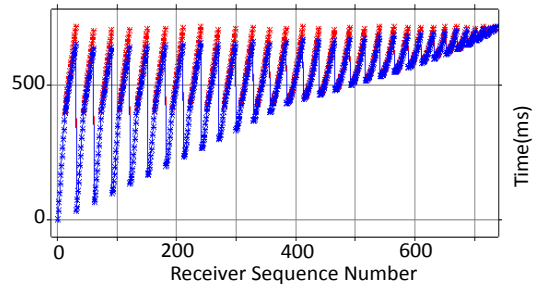

Figure 2: Traveltimes of isotropic and anisotropic velocity model by raytracing from a single shot. Blue denotes traveltimes of anisotropic model and red denotes traveltimes of isotropic model.

Our objective is to understand what happens if we invert the near-surface velocity structures with isotropic medium assumption while the actual model includes HTI anisotropy. Therefore we take the calculated traveltimes from anisotropic model A as input data, and perform the first arrival isotropic traveltime tomography. After 10 iterations, traveltimes associated with the final isotropic tomographic results can match the input data well. This data matching is consistent over all shots which implies with anisotropy in the lower medium, there is no difficulty to fit the data with so many sources and receivers under isotropic assumption.

Figure 3 shows velocity comparisons between two tomography results. (a) depicts horizontal depth slices of the results with HTI refractor (half a space) in the true model but with isotropic tomography applied, and (b) shows the same depth slices but for a true isotropic model and with isotropic tomography applied. The results clearly illustrate that high velocity artifacts are produced in the first case along X axis. It shows a pattern along the anisotropic velocity long axis and following receiver geometry.

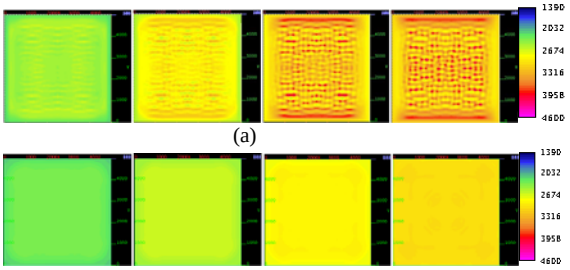

(a)

(b)

Figure 3: With input data with (above) and without HTI anisotropy (below), isotropic traveltime tomography reveals results different. In the first case, HTI anisotropy data leads to artifacts associated with HTI symmetry axis and receiver geometry.

For HTI anisotropic model A, the long offset recording exhibits the first-arrival traveltimes is faster in the long axis direction due to HTI in the refractor. Therefore, when the isotropic traveltime tomography inversion is applied to fit all of the data, it tends to map high-velocity spots along the receiver lines and compensate the extra speed due to HTI parameters in refractor. Figure 4 shows the side view of the model.

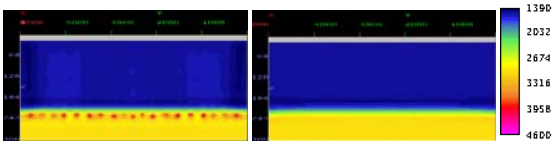

(a) (b)

Figure 4: x=3600m, a) X section of the inversion solution with input HTI data; b) X section of the inversion solution with input isotropic data.

(b) 3D isotropic traveltime tomography for model B

We also design another model B, of which the velocity parameters are the same as the model A, but HTI anisotropy is set in the top layer and the bottom half a space is free of anisotropy. The Comparison of the calculated traveltimes from such a HTI model and traveltimes from isotropic model is shown in Figure 5, and from which it can be seen that both of the near offset (direct waves) and the far offset (refractions) arrivals are affected by anisotropy because of their raypaths through the top layer. Figure 5 depicts that the anisotropic traveltimes (Blue) are faster

DOI http://dx.doi.org/10.1190/segam2012-0907.1

than the isotropic traveltimes (Red) in both short and long offset ranges which suggests that the HTI anisotropy affects both of the direct waves and refractions along Y axis with symmetry axis.

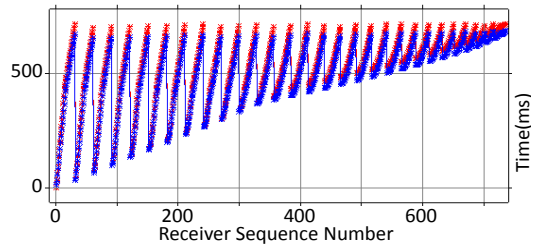

Figure 5: Calculated traveltimes for the HTI velocity model B (blue) and calculated traveltimes for the isotropic velocity model (red).

Similar to the first experiment, we apply the isotropic traveltime tomography to fit the HTI traveltimes, and it has no problem to fit them well. Figure 6 and 7 show the tomographic solutions by using anisotropic traveltimes as input data, along with inversion results from isotropic input data for comparison.

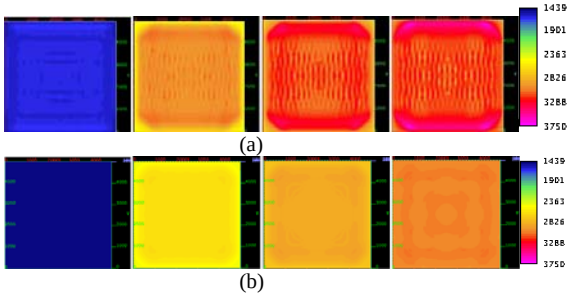

Figure 6: Plan views of velocity solutions by using the HTI input data (a) and the isotropic input data (b).

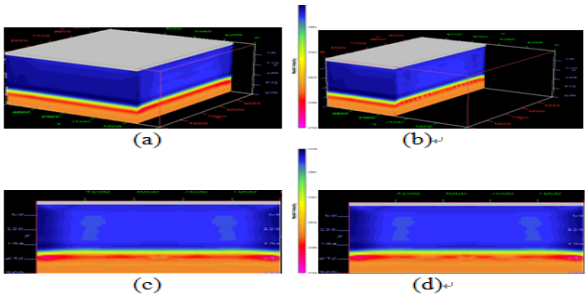

Figure 7: Tomographic inversion results with the HTI data in 3D display, and cross sections. a) and b) show Y cross sections. c) and d) show X cross sections.

Although there is certain minor effect in the top layer, it maps the anomaly due to anisotropy to the bottom layer. That tells the major effect still on the refraction traveltimes.

Anisotropic velocity orientation in synthetic model

In order to observe the geometry's impact on inversion results, we select receivers in the azimuth 0^0, 22.5^0, 45^0, 67.5^0, 90^0, 112.5^0, 135^0,157.5^0, and use the subset of the traveltime data to invert the model, respectively, finally, 8 traveltime tomographic solutions are obtained. By using the inversion results we are able to calculate the fast, slow velocity model and the corresponding anisotropic vector maps. Figure 8 shows the results of model A, as can be seen that the slow velocity model is close to the true model, and the corresponding anisotropic vector direction is the anisotropic symmetry axis, while the anisotropic vector direction corresponding to the fast velocity model is the anisotropic velocity long axis.

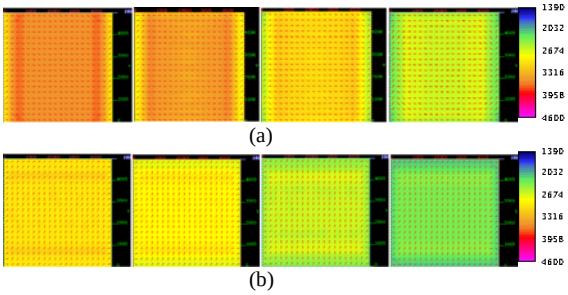

Figure 8: (a) is the fast velocity model and the corresponding anisotropic vector; (b) is slow velocity model and the corresponding anisotropic vector.

Application to real 3D seismic data

In order to further observe anisotropic effects on the near-surface imaging, we select a real datset from a mountain area. The geometry of sources and receivers is shown in Figure 9. The red points represent the distribution of sources, and the yellow points denote receivers' distribution. The total number of sources is 1312. Figure 10 shows a shot gather.

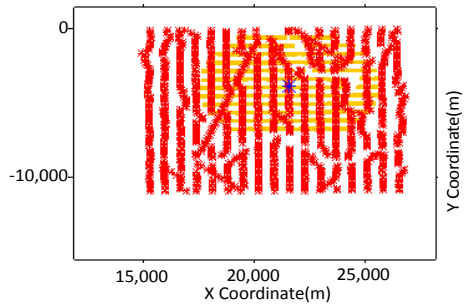

Figure 9: source and receive geometry.

Using an automatic picker, we obtained the first arrival traveltimes of all the shot gathers. Figure 11 is an example of traveltimes of a single shot. By applying the isotropic traveltime tomography method, we obtained a velocity

DOI http://dx.doi.org/10.1190/segam2012-0907.1

model shown in Figure 12. Through the study of the real 3D data, we observed the similar phenomenon to our numerical tests.

In order to understand the anisotropic velocity orientation, we shall calculate azimuthal isotropic tomography with the receiver azimuth 0^0, 22.5^0, 45^0, 67.5^0, 90^0, 112.5^0, 135^0, 157.5^0, similarly to the tests on the synthetic models. Figure 13 shows the results with fast and slow velocity models and corresponding anisotropic vector maps. From fast/slow velocity models and corresponding anisotropic vector maps we can not only get the knowledge of the velocity distribution direction in the depth, but can get a conclusion that anisotropy exists in the near surface area, moreover the results are helpful to determine the direction of the axis of symmetry roughly. In this case we can determine the angle between symmetry axis and x axis is 45^0.

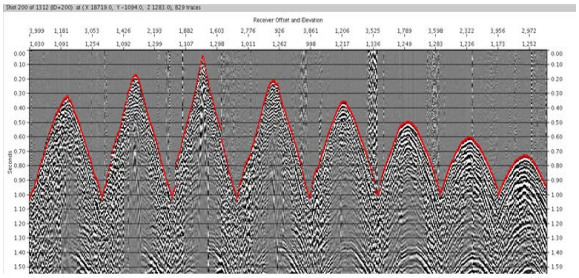

Figure 10: A shot gather.

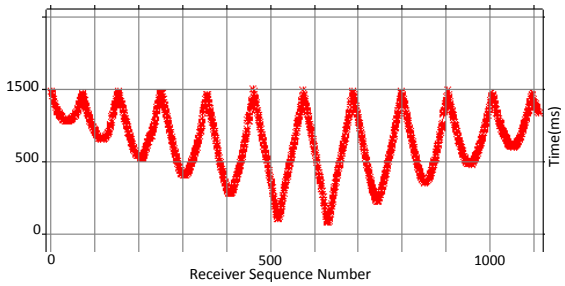

Figure 11: The Picked first arrival traveltimes.

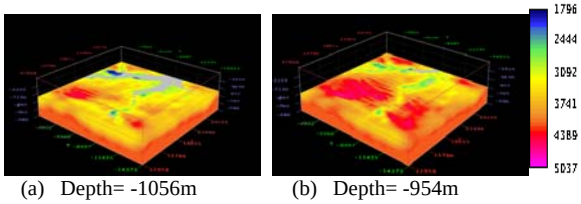

(a) Depth= -1056m (b) Depth= -954m

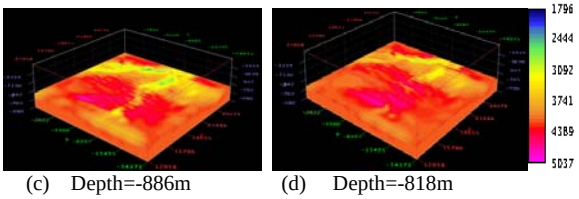

(c) Depth=-886m (d) Depth=-818m

Figure 12: Plan view of 3D isotropic traveltime tomography result.

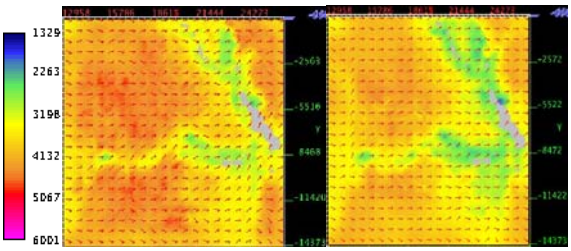

(a) (b)

Figure 13: the section depth is *z=-954m*. (a) is the fast velocity model depth section and fracture vector map; (b) is the slow velocity model and fracture vector map.

Conclusions

We design two simple velocity models with HTI anisotropy included to explore the influence of HTI anisotropy on the results of near surface imaging. In both cases, numerical tests suggest it tends to map anomaly due to anisotropy to the lower layer where more refraction raypaths are available and velocity artifacts are produced. The pattern of the artifacts seems associated with the anisotropic velocity axis and the recording geometry as well, the results of the slow velocity model and corresponding fracture vector direction imply the anisotropic symmetry axis direction and the real velocity range. At the same time, we process a real data that includes anisotropy in the near surface area. From the results of real data, we obtain similar footprint velocity artifact as the test results. This pattern in the imaging results may serve as an approach to identify if any anisotropic effect is significant in the near surface area. Furthermore, combined with slow velocity model the anisotropic vector is helpful to determine the direction of symmetry axis roughly.

Acknowledgments

We appreciate the support from GeoTomo, allowing us to use TomoPlus and VECON software packages to perform this study.

DOI http://dx.doi.org/10.1190/segam2012-0907.1

http://dx.doi.org/10.1190/segam2012-0907.1

EDITED REFERENCES

Note: This reference list is a copy-edited version of the reference list submitted by the author. Reference lists for the 2012 SEG Technical Program Expanded Abstracts have been copy edited so that references provided with the online metadata for each paper will achieve a high degree of linking to cited sources that appear on the Web.

REFERENCES

Bai, C. Y., S. Greenhalgh, and B. Zhou, 2007, 3D ray tracing using a modified shortest-path method: Geophysics, **72**, no. 4, T27–T36.

Helbig, K., and L. Thomsen, 2005, 75–plus years of anisotropy in exploration and reservoir seismics: A historical review of concepts and methods: Geophysics, **70**, no. 6, 9ND–23ND.

McCollum, B., and F. Snell, 1932, Asymmetry of sound velocity in stratified formations: Journal of Applied Physics, **2**, 174–185.

Tsvankin, I., J. Gaiser, V. Grechka, M. Baan, and L. Thomsen, 2010, Seismic anisotropy in exploration and reservoir characterization: An overview: Geophysics, **75**, no. 5, 75A15–75A29.

Zhang, J., and N. Toksoz, 1998, Nonlinear refraction traveltime tomography: Geophysics, **63**, no. 5, 1726–1737.

Zhou, B., and S. A. Greenhalgh, 2005, Shortest path ray tracing for the most general 2D/3D anisotropic media: Journal of Geophysical Engineering, **2**, 54–63.